Crystal Structure, Chemical Bonding, and Magnetic Hyperfine Interactions in $GdRu_2SiC$

Thomas Fickenscher,[†] Sudhindra Rayaprol,[†] Jörg von Appen,[‡] Richard Dronskowski,*[,‡] Rainer Pöttgen,*[,†] Kazimierz Łatka,*[,§] and Jacek Gurgul[△]

Institut für Anorganische and Analytische Chemie, Universität Münster, Corrensstrasse 30, D-48149 Münster, Germany, Institut für Anorganische Chemie, Rheinisch-Westfälische Technische Hochschule Aachen, Landoltweg 1, D-52056 Aachen, Germany, Marian Smoluchowski Institute of Physics, Jagiellonian University, Reymonta 4, 30-059 Kraków, Poland, and Institute of Catalysis and Surface Chemistry, Polish Academy of Sciences, Niezapominajek 8, 30-239 Kraków, Poland

Received July 27, 2007. Revised Manuscript Received October 9, 2007

The silicide carbide $GdRu_2SiC$ was synthesized by arc-melting from the Laves phase $GdRu_2$, silicon, and graphite. $GdRu_2SiC$ was characterized via X-ray powder and single-crystal data: $DyFe_2SiC$ type, *Cmcm*, $a = 383.0(1)$ pm, $b = 1106.9(2)$ pm, $c = 715.7(1)$ pm, wR2 = 0.0363, 626 F^2 values, and 20 variables. The silicon atoms have a distorted trigonal prismatic Gd_2Ru_4 coordination and the carbon atoms fill compressed $[Gd_4Ru_2]$ octahedra. The shortest interatomic distances and strongest bondings occur for the Ru−C (187 pm) and Ru−Si (247 pm) contacts, the former ones even exhibiting double-bond strength. Together, these atoms build up a three-dimensional $[Ru_2SiC]$ network in which the gadolinium atoms fill channels. The magnetic and electronic properties of $GdRu_2SiC$ have been investigated by means of magnetometric and ^{155}Gd Mössbauer spectroscopy measurements. Magnetic susceptibility measurements exhibit magnetic ordering with a broad feature around 10 K. Susceptibility increases below the broad peak, indicating complex magnetism in this compound. This fact is supported by Mössbauer spectroscopy, which exhibits a dramatic change of the Mössbauer spectrum below 4.2 K, indicating another magnetic phase transition. The results of Mössbauer spectroscopy are discussed here in detail to understand the nature of the magnetic ordering in $GdRu_2SiC$ below and above 4.2 K.

Introduction

The Re_3B type structure[1] has more than 100 binary and ternary representatives.[2,3] Besides typical interstitial compounds like Re_3B itself, a large variety of alkaline earth (AE) and rare earth (RE) transition metal (T) aluminides, gallides, indides, and thallides (X) $AETX_2$ and $RETX_2$ have been reported. The AE (RE) and X atoms occupy the two crystallographically independent rhenium sites and the smaller transition metal atoms fill the trigonal AE_2X_4 and RE_2X_4 prisms. Within the $AETX_2$ and $RETX_2$ compounds, the X atoms build up distorted lonsdaleite (hexagonal diamond) related networks with a distorted tetrahedral coordination. This peculiar atomic arrangement has first been observed for $MgCuAl_2$.[4,5] Chemical bonding peculiarities in this family of intermetallics have been discussed in a recent review.[3]

Besides the trigonal prismatic voids filled by the boron atoms, the Re_3B type structure also leaves some octahedral voids that are empty in the prototype. More detailed investigations of other intermetallics like Zr_3Fe,[6] however, revealed oxygen atoms on these sites.[7] Similar behavior was also observed for $DyFe_2SiC$,[8] were the dysprosium and iron atoms build up trigonal prisms $[Dy_2Fe_4]$ that are filled by silicon and the carbon atoms fully occupy the octahedral voids. Sometime later, a whole series of silicide carbide and phosphide carbides with filled Re_3B structure has been reported.[9–12] So far, only some structural data on these intermetallics have been reported. Chemical bonding in $ThFe_2SiC$ has been investigated on the basis of extended Hückel tight binding calculations.[13]

In the course of our systematic studies of magnetic and magnetocaloric properties of gadolinium based interme-

* To whom correspondence should be addressed. E-mail: drons@HAL9000.ac.rwth-aachen.de (R.D.); pottgen@uni-muenster.de (R.P); uflatka@cyf-kr.edu.pl (K.L.).
[†] Universität Münster.
[‡] Rheinisch-Westfälische Technische Hochschule Aachen.
[§] Jagiellonian University.
[△] Polish Academy of Sciences.

(1) Aronsson, B.; Bäckman, M.; Rundqvist, S. *Acta Chem. Scand.* **1960**, *14*, 1001.
(2) Villars, P.; Calvert, L. D. *Pearson's Handbook of Crystallographic Data for Intermetallic Phases*, 2nd ed.; American Society for Metals: Materials Park, OH, 1991,and desk edition, 1997.
(3) Pöttgen, R.; Lukachuk, M.; Hoffmann, R.-D. *Z. Kristallogr.* **2006**, *221*, 435.
(4) Perlitz, H.; Westgren, A. *Ark. Kemi, Miner. Geol.* **1943**, *16B*, 1.
(5) Heying, B.; Hoffmann, R.-D.; Pöttgen, R. *Z. Naturforsch.* **2005**, *60b*, 491.
(6) Matković, P.; Matković, T.; Vicković, I. *(Metalurgija Zagreb, Croatia)* **1990**, *29*, 3.
(7) Mackay, R.; Franzen, H. F. *J. Alloys Compd.* **1992**, *186*, L7.
(8) Paccard, L.; Paccard, D.; Bertrand, Ch. *J. Less-Common Met* **1987**, *135*, L5.
(9) Witte, A. M.; Jeitschko, W. *J. Solid State Chem.* **1994**, *112*, 232.
(10) Witte, A. M.; Jeitschko, W. *Z. Kristallogr. Suppl.* **1995**, *9*, 250.
(11) Hüfken, Th.; Witte, A. M.; Jeitschko, W. *J. Solid State Chem.* **1999**, *142*, 279.
(12) Jeitschko, W.; Pohlkamp, M. Unpublished results.
(13) Koo, H.-J.; Whangbo, M.-H. *Inorg. Chem.* **1999**, *38*, 2204.

10.1021/cm7020406 CCC: $40.75
Published on Web 01/31/2008

tallics,[14–16] we were interested in the GdT_2SiC compounds. The crystal structure, chemical bonding, magnetic and ^{155}Gd Mössbauer spectroscopic data of $GdRu_2SiC$ are reported herein. So far, $GdRu_2SiC$ was characterized only through a Guinier powder pattern.[11]

Experimental Section

Syntheses. Starting materials for the preparation of $GdRu_2SiC$ were gadolinium ingots (Johnson−Matthey), ruthenium powder (Degussa−Hüls, ca. 200 mesh), silicon lumps (Wacker), and graphite flakes (Alfa Aesar), all with stated purities better than 99.9%. In a first step, pieces of the gadolinium ingot were arc-melted[17] to a small button under an argon atmosphere of ca. 600 mbar. The argon was purified before over titanium sponge (870 K), silica gel, and molecular sieves. The small gadolinium button was then arc-melted with a cold-pressed pellet (∅ 6 mm) of ruthenium powder in the ideal 1:2 atomic ratio, resulting in the Laves phase $GdRu_2$.[18] The $GdRu_2$ button was remelted three times in order to ensure homogeneity.

In a second step, the $GdRu_2$ sample was powdered and mixed with Si powder and graphite flakes in the ideal 1:1:1 ratio and cold-pressed to a pellet. The latter was arc-melted again for three times. Subsequently the sample was sealed in an evacuated silica ampule and annealed for three weeks at 1020 K. $GdRu_2SiC$ was obtained as a polycrystalline, silvery sample that is stable in air for months.

X-ray Investigations. The $GdRu_2SiC$ sample was characterized through a Guinier powder pattern using Cu $K\alpha_1$ radiation and α-quartz ($a = 491.30$ pm, $c = 540.46$ pm) as an internal standard. The Guinier camera was equipped with an image plate system (Fujifilm, BAS-1800). The lattice parameters were obtained by a least-squares refinement of the powder data. The indexing of the diffraction lines was facilitated by an intensity calculation[19] using the positional parameters of the refined structure. Our powder (Table 1) and single-crystal lattice parameters ($a = 382.0(1)$ pm, $b = 1104.0(1)$ pm, $c = 714.0(1)$ pm) are in good agreement with the data reported previously ($a = 382.1(1)$ pm, $b = 1105.5(1)$ pm, $c = 714.5(1)$ pm).[11]

Irregularly shaped single crystals of $GdRu_2SiC$ were isolated from the annealed sample by mechanical fragmentation. The crystals were glued to thin quartz fibers using beeswax and first investigated through Laue photographs on a Buerger camera (equipped with a Fujifilm BAS-1800 image plate system) in order to check their quality for intensity data collection. Intensity data were then collected at room temperature on a Nonius CAD4 four-circle diffractometer with graphite monochromatized Mo Kα radiation ($\lambda = 71.073$ p.m.) and a scintillation counter with pulse-height discrimination. Scans were taken in the $\omega/2\theta$ mode. An absorption correction was applied on the basis of psi-scan data followed by a spherical absorption correction. Relevant crystallographic data and details for the data collection are given in Table 1.

The data set showed Laue symmetry *mmm* and the systematic extinctions were compatible with space group *Cmcm*. The atomic parameters of isotypic $DyRu_2SiC$[11] were taken as starting values and the structure was refined with anisotropic displacement parameters for all atoms using SHELXL-97 (full-matrix least-squares on F^2).[20] Because the single-crystal data of $PrOs_2SiC$ and $ThOs_2SiC$[11] revealed some Si/Os mixing and small defects on the carbon site, the occupancy parameters of all sites were refined in separate series of least-squares cycles. In contrast to the osmium compounds, all sites in $GdRu_2SiC$ were fully occupied within two standard uncertainties. In the final cycles, the ideal occupancies were assumed again. A final difference Fourier synthesis revealed no significant residual peaks. The atomic parameters and interatomic distances are listed in Tables 2 and 3. Further details on the structure refinement are available. Details may be obtained from: Fachinformationszentrum Karlsruhe, D-76344 Eggenstein-Leopoldshafen (Germany), by quoting the Registry No. CSD-418807.

Table 1. Crystal Data and Structure Refinement for $GdRu_2SiC$

empirical formula	$GdRu_2SiC$
molar mass	399.49 g/mol
lattice parameters (powder data)	$a = 383.0(1)$ pm
	$b = 1106.9(2)$ pm
	$c = 715.7(1)$ pm
	$V = 0.3034$ nm^3
calculated density	8.75 g/cm^3
space group	*Cmcm*
formula units per cell	$Z = 4$
crystal size	$20 \times 20 \times 40$ μm^3
transmission ratio (max/min)	0.309/0.210
absorption coefficient	31.5 mm^{-1}
$F(000)$	688
θ range for data collection	3−45°
range in *hkl*	±6, ±19, ±14
total no. of reflections	3929
no. of independent reflections	626 ($R_{int} = 0.0382$)
reflections with $I > 2\sigma(I)$	552 ($R_{sigma} = 0.0204$)
data/parameters	626/20
GOF on F^2	1.130
final R indices [$I > 2\sigma(I)$]	R1 = 0.0179
	wR2 = 0.0346
R indices (all data)	R1 = 0.0242
	wR2 = 0.0363
extinction coefficient	0.0054(2)
largest diff. peak and hole	2.57 and −1.92 e/Å^3

Scanning Electron Microscopy. The bulk sample and the investigated single crystal have been analyzed in a LEICA 420 I scanning electron microscope equipped with an OXFORD EDX analyzer. Because the crystal was mounted by beeswax on a glass fiber, it was first coated with a carbon film. GdF_3, Ru, and SiO_2 have been used as standards for the EDX measurements. The experimental setup of the microscope did not allow the determination of the carbon content. The analyses for gadolinium, ruthenium, and silicon were in good agreement with the ideal composition and no impurity elements heavier than sodium have been observed.

Magnetic Susceptibility Measurements. Magnetic measurements (ac and dc magnetization) were performed on a Quantum Design physical property measurement system (PPMS). The powdered sample, enclosed in a gelatine capsule, was fixed to the end of the sample rod. Magnetization was measured as a function of temperature (in 2–300 K) and field (0–80 kOe).

^{155}Gd Mössbauer Spectroscopy. The ^{155}Gd Mössbauer spectroscopy (MS) studies on $GdRu_2SiC$ were performed with a $^{155}Eu:SmPd_3$ (86.5 keV γ-transition) source. A standard constant acceleration spectrometer of the Kankeleit type in the transmission geometry was used. The velocity scale was calibrated at room temperature with a $^{57}Co(Rh)$ source and a metallic iron foil. Spectra

(14) Łątka, K.; Kmieć, R.; Rams, M.; Pacyna, A. W.; Zaremba, V. I.; Pöttgen, R. *Z. Naturforsch.* **2004**, *59b*, 947.
(15) Łątka, K.; Kmieć, R.; Kruk, R.; Pacyna, A. W.; Fickenscher, Th.; Hoffmann, R.-D.; Pöttgen, R. *J. Solid State Chem.* **2005**, *178*, 2077.
(16) Łątka, K.; Kmieć, R.; Pacyna, A. W.; Gurgul, J.; Zaremba, V. I.; Pöttgen, R. *Solid State Sci.* **2006**, *8*, 548.
(17) Pöttgen, R.; Gulden, Th.; Simon, A. *GIT Labor-Fachzeitschrift* **1999**, *43*, 133.
(18) Compton, V. B.; Matthias, B. T. *Acta Crystallogr.* **1959**, *12*, 651.
(19) Yvon, K.; Jeitschko, W.; Parthé, E. *J. Appl. Crystallogr.* **1977**, *10*, 73.
(20) Sheldrick, G. M. *SHELXL-97, Program for Crystal Structure Refinement*; University of Göttingen: Göttingen, Germany, 1997.

Table 2. Atomic Coordinates and Anisotropic Displacement Parameters (pm^2) for $GdRu_2SiC$[a]

atom	Wyckoff site	*x*	*y*	*z*	U_{11}	U_{22}	U_{33}	U_{23}	U_{eq}
Gd	4*c*	0	0.04809(2)	1/4	56(1)	52(1)	67(1)	0	58(1)
Ru	8*f*	0	0.66488(2)	0.55762(4)	60(1)	43(1)	54(1)	−2(1)	52(1)
Si	4*c*	0	0.76927(13)	1/4	61(5)	71(5)	69(5)	0	67(2)
C	4*b*	0	1/2	0	85(16)	49(15)	76(15)	6(12)	70(6)

[a] U_{eq} is defined as one-third of the trace of the orthogonalized U_{ij} tensor. $U_{12} = U_{13} = 0$.

Table 3. Interatomic Distances (pm) in the Structure of $GdRu_2SiC$, Calculated with the Lattice Parameters Taken from X-Ray Powder Data[a]

Gd	4	C	267.4(1)	Ru	1	C	187.1(1)
	1	Si	308.6(2)		2	Si	246.9(1)
	2	Si	310.8(1)		1	Si	248.6(1)
	4	Ru	319.2(1)		1	Ru	275.4(1)
	4	Ru	333.5(1)		2	Ru	281.0(1)
	2	Ru	346.3(1)		2	Gd	319.2(1)
	2	Gd	373.4(1)		2	Gd	333.5(1)
	2	Gd	383.0(1)		1	Gd	346.3(1)
Si	4	Ru	246.9(1)	C	4	Ru	187.1(1)
	2	Ru	248.6(1)		2	Gd	267.4(1)
	1	Gd	308.6(2)				
	2	Gd	310.8(1)				

[a] Standard deviations are given in parentheses. All distances within the first coordination spheres are listed.

were recorded in a liquid helium cryostat at temperatures between 2.15 and 15 K. During measurements, the temperature of the source was close to 4.2 K.

The absorber was prepared from the fine powdered compound with an optimized thickness[21] equal to 368 mg/cm^2. Resonance transition was detected using a germanium detector. A 0.9 mm thick lead foil was applied as a critical absorber to reduce the background intensity. The isomer shift values are given relative to the source material.

Because the gadolinium sites have a rather low symmetry (*m*2*m*), i.e., two mutually perpendicular mirror planes, diagonalization of the complete hyperfine interaction Hamiltonian[22] was used to determine the hyperfine parameters. The Hamiltonian written in the principal axis system of the electric field gradient tensor (EFG) is given by the formula

$$\hat{H} = -g\mu_B H_{hf}\left[\hat{I}_z\cos\theta + \frac{1}{2}(\hat{I}_+ e^{-i\varphi} + \hat{I}_- e^{-i\varphi})\right] + \frac{\Delta E_Q}{4I(2I-1)}[3\hat{I}_z - \hat{I}^2 + \frac{n}{2}(\hat{I}_+^2 + \hat{I}_-^2)] \quad (1)$$

where H_{hf} is the magnetic hyperfine field at the nuclear site; $\Delta E_Q = eV_{zz}Q$ is the quadrupole interaction constant, V_{zz} is the z-component of the EFG tensor, and Q is the quadrupole moment of the nuclear state; η is the asymmetry parameter defined as $\eta = (V_{xx} - V_{yy})/V_{zz}$, θ is the angle between the direction of H_{hf}, and the V_{zz} axis, Φ is the angle between the V_{xx} axis and projection of H_{hf} onto the *xy* plane. If the principal axes are chosen in the form $|V_{xx}| < |V_{yy}| < |V_{zz}|$, then $0 \le \eta \le 1$.

From a spectrum obtained in the paramagnetic state only the effective absolute quadrupole interaction value $|E_Q^{eff}| = |eQV_{zz}|\cdot(1 + \eta^2/3)^{1/2}$ can be inferred, because of the small magnitude of the excited quadrupole moment.[23] In contrast, magnetic hyperfine split spectra have to be fitted with independent $\Delta E_Q = eQV_{zz}$ and η parameters in self-consistent way because they are usually correlated.

A transmission integral formula was applied to describe the resonance lineshapes. For ^{155}Gd studies, the source line width Γ_S and the background reduced Debye–Waller factor f_S of the source were obtained from the independent measurement with a standard $GdFe_2$ absorber, where the natural line width $\Gamma_{nat} = 0.25$ mm/s was assumed.[23] The Debye–Waller factor f_A was fitted as an independent parameter. During the analysis, the g factor and the quadrupole-moment ratios were constrained as equal to $g_{ex}/g_g = 1.235$ and $Q_{ex}/Q_g = 0.087$, respectively.[24] In the analysis of ^{155}Gd spectra, an interference ζ factor for the $E_\gamma = 86.5$ keV gamma transition in the ^{155}Gd nuclei was fixed to the value $\zeta = 0.0275$.[22,25] To properly fit the resonance spectrum recorded at $T = 2.15$ K, we employed the Wivel and Mørup method,[26] which takes into account a broad quasi-continuous distribution of the magnetic hyperfine fields H_{hf}. The spectra were then least-squares fitted with 50 values of H_{hf}, giving the probability distribution curve $F(H_{hf})$.

Electronic Structure Calculations. The first-principles electronic structure calculations of density-functional type were performed using the TB-LMTO-ASA 4.7 program,[27] which is based on all-electron scalar-relativistic linear muffin-tin orbital (LMTO) theory[28–30] in its tight-binding representation.[31] A 16 × 16 × 6 mesh was used for the LMTO calculation of the original unit cell and an 8 × 8 × 16 mesh for the calculation of the magnetic superstructure, which is twice as large. The optional use of empty spheres was avoided by a careful adjustment of the atomic-sphere sizes. The chemical bonding situation was analyzed using the crystal orbital Hamilton population (COHP) technique[32] as implemented in the TB-LMTO-ASA program package.

Results and Discussion

Crystal Chemistry and Chemical Bonding. The structure of the silicide carbide $GdRu_2SiC$ is derived from the well-known Re_3B type. From a geometrical point of view, the gadolinium and ruthenium atoms build up distorted trigonal prisms that are filled by the silicon atoms (Figure 1). Here, the gadolinium and ruthenium positions correspond to the two crystallographically independent rhenium sites, and the silicon atoms are located on the boron site. In contrast to the Re_3B type intermetallics, in $GdRu_2SiC$, the octahedral voids formed by the gadolinium and ruthenium atoms are completely filled by carbon atoms.

The carbon-centered $[Gd_4Ru_2]$ octahedra are compressed. Because of the different radii of gadolinium and ruthenium,

(21) Long, G. J.; Cranshaw, T. E.; Longworth, G. *Mössbauer Eff. Ref. Data J.* **1983**, *6*, 42.
(22) Tomala, K.; Czjzek, G.; Fink, J.; Schmidt, H. *Solid State Commun.* **1977**, *24*, 857.
(23) Czjzek, G. Mössbauer Spectroscopy of New Materials Containing Gadolinium. In *Mössbauer Spectroscopy Applied to Magnetism and Materials Science*; Long, G. J., Grandjean F., Eds.; Plenum Press: New York, 1993, p 373.; Vol. 1.
(24) Armon, H.; Bauminger, E. R.; Ofer, S. *Phys. Lett.* **1973**, *43B*, 380.
(25) Henning, W.; Baehrle, G.; Kienle, P. *Phys. Lett. B* **1979**, *31*, 203.
(26) Wivel, C.; Mørup, S. *J. Phys. E* **1981**, *14*, 605.
(27) Krier, G.; Jepsen, O.; Burkhardt, A.; Andersen, O. K. *The TB-LMTO-ASA program*, version 4.7; Max-Planck-Institut für Festkörperforschung: Stuttgart, Germany.
(28) Andersen, O. K. *Phys. Rev. B* **1975**, *12*, 3060.
(29) Skriver, H. *The LMTO Method*; Springer: Berlin, 1984.
(30) Andersen, O. K. Linear methods in band theory. In *The Electronic Structure of Complex Systems*; Phariseau, P. W., Temmerman, M., Eds.; Plenum, New York, 1984.
(31) Andersen, O. K.; Jepsen, O. *Phys. Rev. Lett.* **1984**, *53*, 2571.
(32) Dronskowski, R.; Blöchl, P. E. *J. Phys. Chem.* **1993**, *97*, 8617.

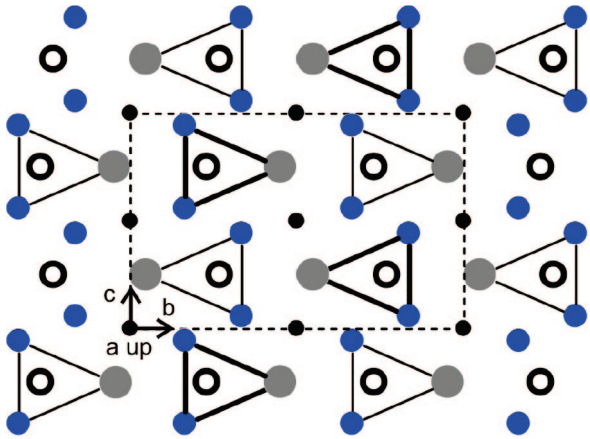

Figure 1. Projection of the $GdRu_2SiC$ structure onto the *yz* plane. The gadolinium, ruthenium, and silicon atoms are drawn as medium grey, blue, and open circles, respectively. All atoms lie on mirror planes at $x = 0$ (thin lines) and $x = 1/2$ (thick lines), respectively.

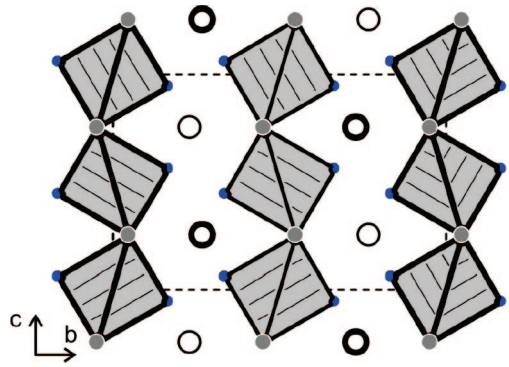

Figure 2. Projection of the $GdRu_2SiC$ structure along the short unit cell axis. The gadolinium, ruthenium, and silicon atoms are drawn as medium grey, blue, and open circles, respectively. The layers of edge-sharing carbon filled $[Ru_2Gd_4]$ octahedra are emphasized. Thin and thick line widths indicate the height difference by *a*/2.

the central carbon atom has shorter C−Ru (187 pm) and longer C−Gd (267 pm) distances. The $[Gd_4Ru_2]$ octahedra are condensed via common edges (Figure 2) in the *ac* direction as well as along the *a* axis. The silicon atoms are located between these layers. They are connected to six ruthenium atoms at Ru−Si distances ranging from 246 to 249 pm, only slightly longer than the sum of the covalent radii[33] of 241 pm. A similar range of Ru−Si distances has also been observed for the silicides $HoRu_2Si_2$ (237 pm),[34] $Er_2Ru_3Si_5$ (237–250 pm), and $Er_2Ru_3Si_{4.6}$ (239–248 pm).[35] Besides the Ru−Si interactions, the layers of edge-sharing octahedra are also condensed via Ru−Ru contacts at a relatively short Ru−Ru bond lengths of 275 and 281 pm, only slightly longer than the average Ru−Ru distance of 268 p.m. in *hcp* ruthenium,[36] and similar to the silicide $Er_2Ru_3Si_5$ (278 pm Ru−Ru).[35]

Considering the short Ru−C and Ru−Si distances, we can assume that these are strongly bonding interactions. Especially the short Ru−C distances of 187 pm are significantly

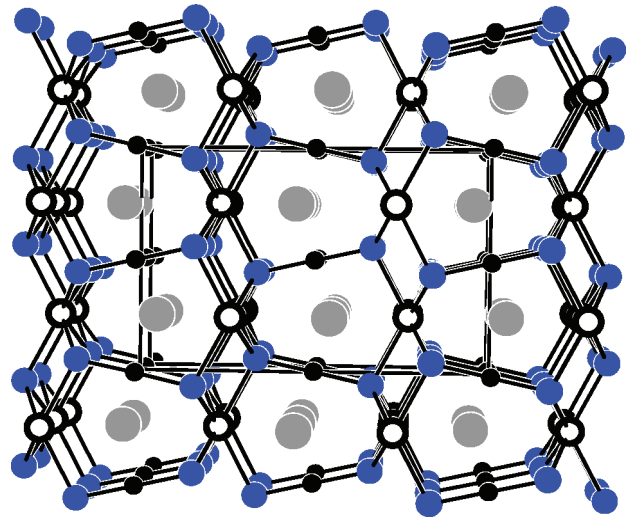

Figure 3. View of the $GdRu_2SiC$ structure approximately along the *x* axis. Gadolinium, ruthenium, silicon, and carbon atoms are drawn as medium grey, blue, black, open and filled circles, respectively. The three-dimensional $[Ru_2SiC]$ network is emphasized.

shorter than the Ru−C distances of 221 and 214 pm. in the two-dimensional $[RuC_4]$ and $[RuC_2]$ polyanions of Sc_3RuC_4[37] and $GdRuC_2$.[38] As emphasized in Figure 3, the ruthenium, silicon, and carbon atoms build up a three-dimensional $[Ru_2SiC]$ polyanionic network that leaves channels for the gadolinium atoms. The main bonding of gadolinium to the $[Ru_2SiC]$ network proceeds through the Gd−C contacts at 267 pm, similar to the structure of $GdRuC_2$ (260 and 261 pm Gd−Ru).[38]

Chemical Bonding Analyses. Because the ground state of the condensed phase $GdRu_2SiC$ exhibits antiferromagnetic ordering (see below), spin-polarized electronic-structure calculations touching upon the correct magnetic structures are mandatory. This information is especially important, because the high nuclear cross-section of natural gadolinium makes neutron diffraction studies useless.

With the objective to theoretically clarify the most stable magnetic structure, we first calculated the most likely magnetic orderings in order to compare their relative stability. Thus, the symmetry of the unit cell had to be lowered and the unit cell was doubled along the *a*-direction such that the former singular crystallographic Gd position could be discriminated into one "spin up" and another "spin down" Gd atom. This led to three different antiferromagnetic orderings that were numerically investigated using space groups *Pbcm* (a), *Amm*2 (b), and *Pnma* (c), as shown in Figure 4. As a reference, we calculated the total energy of a hypothetical nonmagnetic structure, too. The theoretical saturation magnetization, given in Table 4, is independent of the kind of antiferromagnetic ordering, and the local moment has a spin-only value of 6.95 μ_B per Gd atom, 12% smaller than the experimental one. Furthermore, the comparison with a hypothetical nonmagnetic situation give evidence of the enormous stabilization due to spin-polariza-

(33) Emsley, J. *The Elements*; Clarendon Press: Oxford, U.K., 1989.
(34) Horvath, C.; Rogl, P. *Mater. Res. Bull.* **1985**, *20*, 35.
(35) Paccard, D.; Paccard, L. *J. Less-Common Met.* **1990**, *163*, L13.
(36) Donohue, J. *The Structures of the Elements*; Wiley: New York, 1974.
(37) Hoffmann, R.-D.; Pöttgen, R.; Jeitschko, W. *J. Solid State Chem.* **1992**, *99*, 134.
(38) Hoffmann, R.-D.; Wachtmann, K. H.; Ebel, Th.; Jeitschko, W. *J. Solid State Chem.* **1995**, *118*, 158.

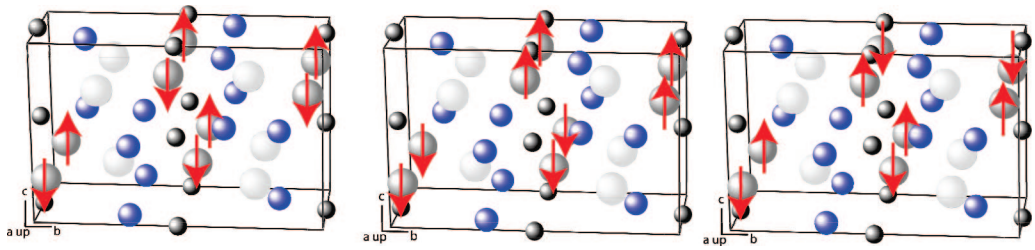

Figure 4. Three possible antiferromagnetic orderings of $GdRu_2SiC$ with the Gd, Ru, Si, and C atoms drawn as medium grey, blue, light-grey, and dark-grey spheres. The red arrows display the spin orientations of the Gd atoms. Type a (left) has been calculated using space group *Pbcm*, type b (middle) using *Amm*2, and type c (right) using *Pnma*.

Table 4. Total Energies and Magnetic Saturation Moments of a Hypothetical Nonmagnetic (NM) $GdRu_2SiC$ and its Three Antiferromagnetic (AFM) Structural Variants Obtained by Density-Functional Theory

type	space group	magnetism	ΔE (eV)	$\mu(\mu_B)$
nonmagnetic	*Cmcm*	NM	0	
A	*Amm*2	AFM	−7.52	6.95
B	*Pbcm*	AFM	−7.50	6.95
C	*Pnma*	AFM	−7.64	6.95

tion in combination with antiferromagnetism for this compound, also almost independent of the individual orderings. In particular, Table 4 yields an energetic gain of at least 7.5 eV per formula unit for any antiferromagnetic type. The most stable one is the arrangement of type (c), in which the spins change their direction both inside the chains in the *a*-direction (Gd−Gd distance: 3.83 Å) and between the neighboring chains in *b*-direction (3.73 Å).

Therefore, the chemical bonding analysis refers to this most stable "doubled" antiferromagnetic structure (c). Nonetheless, we note that the DOS and COHP curves of the two other antiferromagnetic candidates differ just marginally. Most prominent in the DOS (Figure 5) are the two large and narrow peaks of the Gd atoms indicating the site-bonded character of the electrons inside the 4f orbitals. The deep-lying states at −11 eV are mainly made up by the carbon 2s orbitals, and those at −8 eV refer to the silicon 3*s*-orbitals. The higher states between −5 eV and the Fermi level are mainly due to ruthenium and gadolinium d-contributions as well as carbon and silicon p-orbitals.

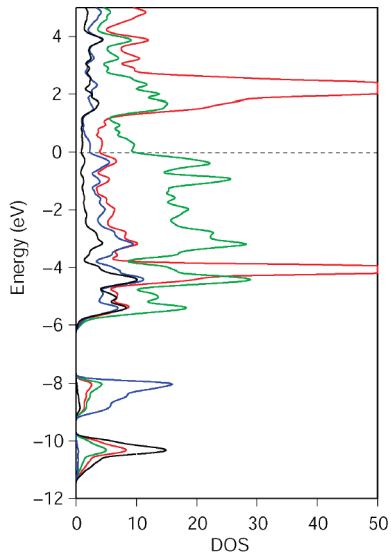

Figure 5. Total and local densities of states (DOS) in $GdRu_2SiC$ highlighting the contributions of Gd (red), Ru (green), Si (blue), and C (black).

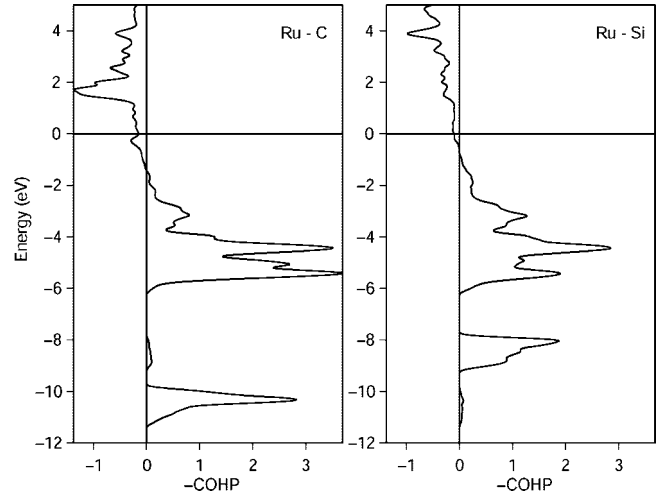

Figure 6. Crystal orbital Hamilton populations (COHP) of the Ru−C (left) and the Ru−Si interactions in $GdRu_2SiC$.

The COHP curves in Figure 6 display the two most important bonding interactions, namely the Ru−C (left) and Ru−Si (right) contacts. Both COHPs evidence the deep-lying attractive interaction between Ru and carbon/silicon s-orbitals and also the higher-lying ones between Ru and the carbon/silicon p-orbitals. The integrated COHP (ICOHP), equivalent with the covalent contribution to the band-structure energy (sum of the Kohn–Sham orbital energies), amounts to −6.6 eV (ca. −637 kJ/mol) for every Ru−C bond, significantly more than what is to be expected for a single bond. For the Ru−Si bond, on the other side, the energy is −2.0 eV (−193 kJ/mol). Thus, these interactions within the polyanionic network represent the leading terms for the cohesive energy of this compound. In addition, there are further attractive interactions between Ru−Ru and Gd−C (COHPs not shown for reasons of brevity) but these tend out to be much weaker, e.g., with a maximum ICOHP of −1 eV for a Ru−Ru interaction. The extraordinarily strong Ru−C bond can also be visualized in terms of the calculated electron density, and a corresponding plot is given in Figure 7. Here, the Ru−C bond clearly exhibits the largest (red) electron-density value.

Magnetic Properties. The magnetic susceptibility, χ (= M/H) of $GdRu_2SiC$ measured under 10 kOe applied field is plotted in the mainframe of Figure 8. χ increases continuously with decreasing temperature, behaving as a paramagnet. Around 10 K, the $\chi(T)$ exhibits a broad peak, indicating antiferromagnetic type ordering (see the insert of Figure 8). Interestingly, below 10 K, $\chi(T)$ increases up to 2 K, indicating complex magnetic nature. The inverse susceptibility behavior

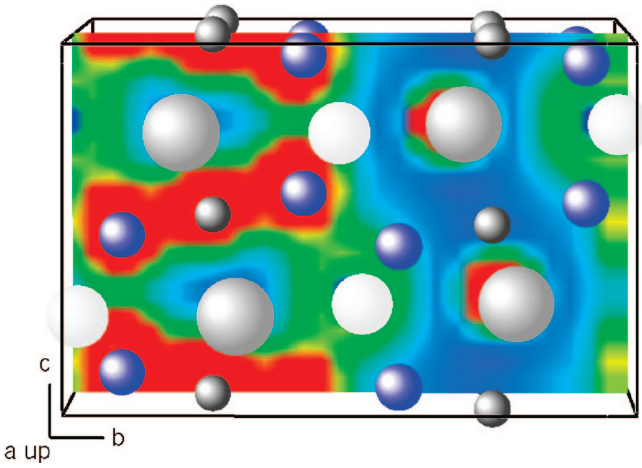

Figure 7. Electron density of $GdRu_2SiC$ in the *yz*-plane at $x = 0$ with the Gd, Ru, Si, and C atoms drawn as medium-grey, blue, light-grey, and dark-grey spheres. At $x = 1/2$, one finds the same structural situation, but translated by 1/2 along *y*. The electron density increases from blue to red.

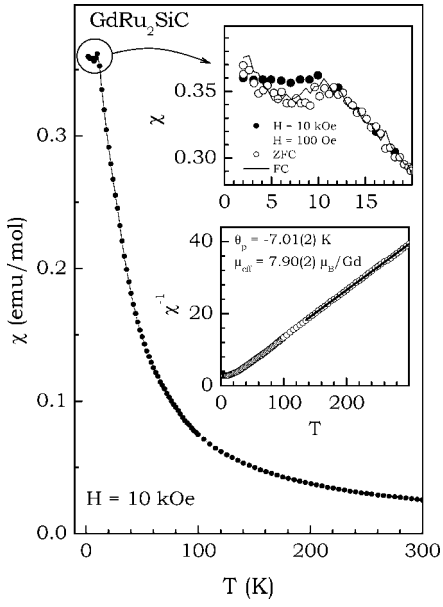

Figure 8. Magnetic susceptibility ($\chi = M/H$) of $GdRu_2SiC$ measured in an applied field of 10 kOe after zero-field-cooling of the sample. The low temperature susceptibility behavior is shown in an expanded scale in the top insert along with χ measured at low field in ZFC and FC state of the sample. The second insert shows the inverse susceptibility behavior of a 10 kOe measurement. The straight line passing through the data points is drawn to show the linear region for fitting the Curie–Weiss law.

is also shown in the same figure. The $\chi(T)$ follows Curie–Weiss law above 100 K. From the linear fit in the paramagnetic region, the paramagnetic Curie temperature (θ_p) of $-7.0(1)$ K is obtained which is close to T_N, indicating long-range magnetic ordering in $GdRu_2SiC$. The negative sign is indicative for antiferromagnetic interactions. Hence, we refer the ordering temperature at 10 K as the Neél temperature (T_N). The effective Bohr magneton number (μ_B) obtained from the linear fit, 7.90(2) μ_B/Gd, is also close to the expected value of 7.94 μ_B for Gd^{3+}.

To probe the increase in χ below T_N, we have measured χ(T) at a smaller field of 100 Oe in the zero field cooled (ZFC) and field cooled (FC) state of the sample. The data

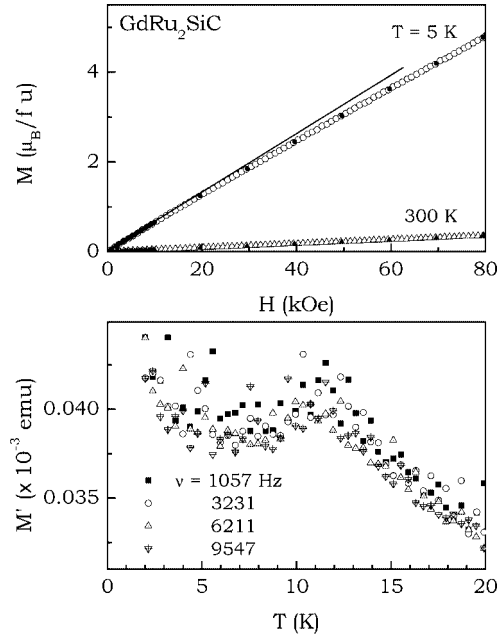

Figure 9. Top: Magnetization (M) vs field (H) of $GdRu_2SiC$ at 5 and 300 K. The straight line is drawn through the origin to highlight the deviation of the 5 K curve around 20 kOe. The up and down magnetization cycles are shown by open and filled symbols respectively. Bottom: ac susceptibility of $GdRu_2SiC$ measured at different driving frequencies and an ac amplitude of 1 Oe.

are plotted in the insert of Figure 8. The important point to consider here is that the absence of bifurcation in the ZFC-FC curves rules out any spin-glass anomalies. The increase of χ(T) is clearly visible at this low field measurement also. It is also interesting to note that the moment value is independent of the applied field.

We have also measured ac susceptibility of $GdRu_2SiC$ with ac amplitude of 1 Oe at different driving frequencies (Figure 9). There is no frequency dependence around the peak temperature, however the features of χ(T) seen in dc χ measurements are confirmed here also. There is a broad peak around 10 K for all frequencies, and susceptibility increases below the peak temperature. Magnetization (M) as a function of ramping field (H) is also plotted in Figure 9. At 5 K, M increases linearly with H as if the compound is a paramagnet, however at close examination, the M(H) curve at 5 K is not linear, the curve deviates slightly around 20 kOe, however there is no hysteresis at low fields ruling out any spin-glass like behavior. M(H) at 300 K clearly shows the paramagnetic behavior.

Considering the ac and dc magnetization data together, $GdRu_2SiC$ undergoes antiferromagnetic ordering of long-range type at 10 K with another magnetic structure evolving in the ordered region (below 10 K), which is discussed in detail below.

^{155}Gd Mössbauer spectroscopy. To correctly interpret the Mössbauer data and to get some information on the magnetic structure of $GdRu_2SiC$, one must consider the relation between the local symmetry of the gadolinium site and the hyperfine parameters. The unit cell of $GdRu_2SiC$ contains four equivalent gadolinium ions. The only local symmetry elements at the gadolinium sites are two mutually perpendicular mirror planes, where one of the planes lies in

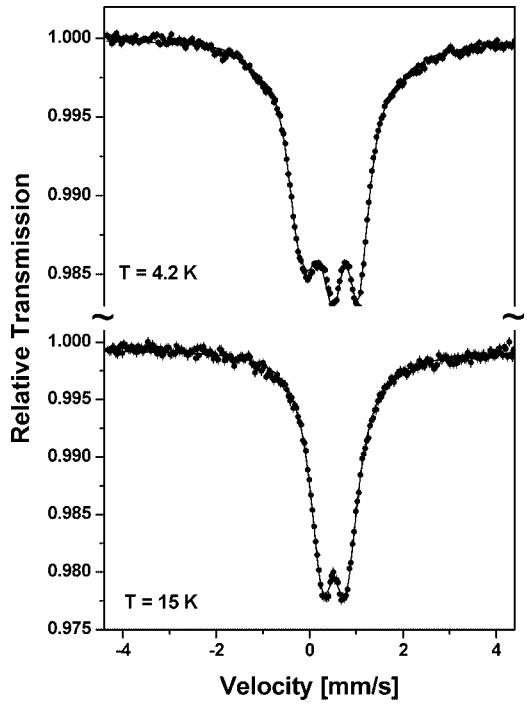

Figure 10. ^{155}Gd resonance spectra for $GdRu_2SiC$ at $T = 15$ and 4.2 K. The continuous line represents the least-squares fit to the experimental points.

the **bc**-basal plane and the second one is parallel to the crystallographic **a**-axis. Due to this arrangement, one of the principal axes of the EFG tensor has to be parallel to the **a**-axis and two others have to lie in the basal plane, with one of them parallel to the cross-section of the mirror planes. In our case, all principal axes of the EFG tensor coincide with the crystallographic axes. The assignment of the individual principal axes of the EFG to specific crystallographic axes, however, remains open. With each of the four gadolinium positions in the unit cell are associated four different principal systems of axes of the EFG tensor, which are equivalent after rotation around the **a**-axis by 90°.

In light of the above considerations, the four magnetically split components can be related to the four principal axes of the EFG at the gadolinium sites in the unit cell. A single component observed in the paramagnetic state reflects the crystallographic equivalence of the gadolinium position. Generally, for any noncollinear magnetic structure, the magnetically split $GdRu_2SiC$ spectrum could be either a single or a multicomponent one. The symmetry of the crystallographic structure determines, however, that any collinear alignment of the gadolinium magnetic moments not parallel to the **a**-axis would give four different components in the magnetically split Mössbauer spectra. The spectra would have the same intensities, magnitudes of H_{hf}, ΔE_Q, δ_{is}, and η parameters but different θ and φ angles. In the case when all the gadolinium magnetic moments were parallel to the crystallographic **a**-axis, one would expect just a single component in the resonance spectrum. Because our spectra for $T \geq 4.2$ K (Figure 10) can be very well fitted with only one component, and hence we believe that magnetic moments in our sample are parallel to the crystallographic **a**-axis and the magnetic structure is collinear. To get reliable information concerning the hyperfine parameters and the orientation of the EFG tensor with respect to the crystallographic axes, under the assumption that indeed the magnetic moments are ordered collinearly along the **a**-axis, one has to consider in the fitting strategy of magnetically split spectra six possible sets of the θ and φ angles, including two possible signs of the V_{ii}, namely

(1) for the $\pm V_{zz}$ axis parallel to the **a**-axis, $\theta = 0°$ and φ is indefinite,

(2) for the $\pm V_{xx}$ axis parallel to the **a**-axis, $\theta = 90°$ and $\varphi = 0°$,

(3) for $\pm V_{yy}$ axis parallel to the **a**-axis, $\theta = 90°$ and $\varphi = 90°$.

Because one could obtain a good quality fit (see Table 4) with the asymmetry parameter η in the required range $0 \leq \eta \leq 1$ only for a negative V_{zz} value, $\theta = 90°$ and $\varphi = 0°$, one can conclude that the V_{xx} axis of the EFG tensor coincides with the **a**-axis and the other two components of the EFG tensor lie in the **bc**-basal plane (Figure 1). It is worthwhile to note that simple point charge model calculations confirm that the main axes of the EFG are oriented along the crystallographic axes giving just negative value of V_{zz}.

The trivalent gadolinium ion in the $^8S_{7/2}$ electronic state with a spherical distribution of the 4*f* electronic charge is insensitive to crystal field effects (CFE), and consequently ^{155}Gd nuclei are a good probe for a lattice contribution to the electric field gradient. Hence, the determination of the sign and magnitude of $\Delta E_Q = eV_{zz}Q$ at the gadolinium site together with the asymmetry parameter η allow to estimate the quadrupolar terms B_2^0 and B_2^2 in the Stevens expansion of the crystal field Hamiltonian $\Sigma B_n^m O_n^m$, as they are directly related by two simple formulas: $B_2^0\,[K] = -a_J <r^2>_{4f} 90.25\ \Delta E_Q(^{155}\text{Gd})$ and $B_2^2 = \eta B_2^0$.

Here, a_J is the appropriate Stevens factor, the mean squared radius of the 4f wave function $<r^2>_{4f}$ is expressed in atomic units and ΔE_Q in mm/s ($\Delta E_Q = -1.03$ mm/s; see Table 5). If B_2^0 is the leading term in the crystal field Hamiltonian then its sign gives information about the single ion magnetic anisotropy. Since the measured ΔE_Q is negative, one should expect, for example, a positive value of B_2^0 for isostructural $RERu_2SiC$ compounds with heavy rare earth like Er or Tm ($\alpha_J > 0$), and a negative value of B_2^0 for compounds with light rare earths like Ce, Nd, Pr ($\alpha_J < 0$).

The temperature dependence of the magnetic hyperfine field $|H_{hf}(T)|$ (Figure 11) can be very well described in the framework of a molecular field approximation by a Brillouin function with $S = 7/2$. The resulting fit gives the estimation for the Neél temperature $T_N^{MS} = 10.2(1)$ K which is fairly close to that obtained from magnetic measurements. The absolute value of the saturated magnetic hyperfine field $|H_{hf}(0)|$ is 304(1) kOe. Assuming that the latter value is negative as observed for gadolinium intermetallics[23] and neglecting to a first approximation, the orbital as well as the dipolar contributions to the magnetic hyperfine field H_{hf} at the gadolinium site, one can estimate the contribution of the conduction electron polarization H_{CE}. Following the discus-

Table 5. Hyperfine Interaction Parameters Inferred from the ^{155}Gd Resonance Spectra Obtained for $GdRu_2SiC$ (χ^2 is a fit quality factor)

T (K)	ΔE_Q (mm/s)	δ_{IS} (mm/s)	H_{hf} (kOe)	θ (deg)	φ (deg)	η	Γ_A (mm/s)	χ^2
4.2	−1.03[a]	0.516(3)	273(1)	90(5)	0[a]	0.25(9)	0.25(1)	1.23
5.5	−1.03[a]	0.516(4)	256(1)	93(7)	0[a]	0.25[a]	0.25[a]	0.72
6.5	−1.03[a]	0.511(4)	238(1)	91(5)	0[a]	0.25[a]	0.25[a]	0.59
7.5	−1.03[a]	0.511(4)	214(1)	90(5)	0[a]	0.25[a]	0.25[a]	0.62
8.0	−1.03[a]	0.519(3)	197(1)	98(4)	0[a]	0.25[a]	0.25[a]	0.78
8.5	−1.03[a]	0.517(3)	175(1)	98(5)	0[a]	0.25[a]	0.25[a]	0.68
9.0	−1.03[a]	0.509(4)	136(2)	95(9)	0[a]	0.25[a]	0.25[a]	0.92
9.5	−1.03[a]	0.511(3)	117(3)	93(3)	0[a]	0.25[a]	0.25[a]	0.81
15	1.06(1)[b]	0.522(2)	–	–	–	–	0.26(1)	0.67

[a] Parameters kept constant during the fit. [b] Here, $\Delta E_Q = |\Delta E_Q^{eff}|$ as described in the main text.

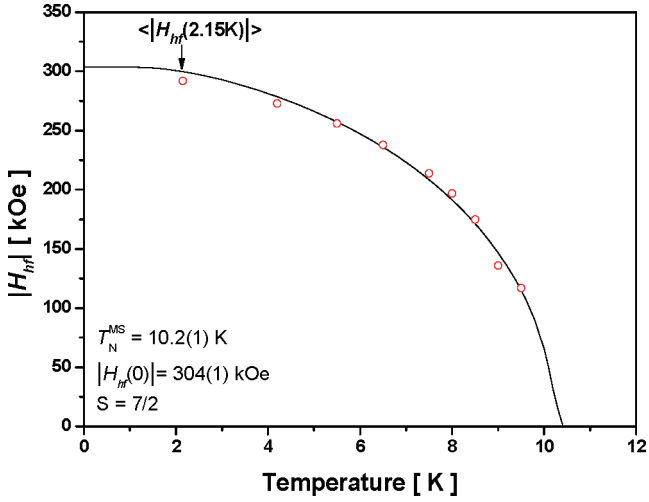

Figure 11. Temperature evolution of the magnetic hyperfine field $|H_{hf}|$ at the gadolinium site of $GdRu_2SiC$. The continuous line represents the least-squares fit of the Brillouin function for $S = 7/2$. The fit gives the estimated Néel temperature $T_N^{MS} = 10.2(1)$ K and the absolute value of the saturated magnetic hyperfine field $|H_{hf}(0)| = 304(1)$ kOe. The point at $T = 2.15$ K marked by the arrow was added after fit and represents the average magnetic hyperfine field $|H_{hf}(2.15)|$ evaluated from the derived distribution of magnetic hyperfine fields (for explanation see text).

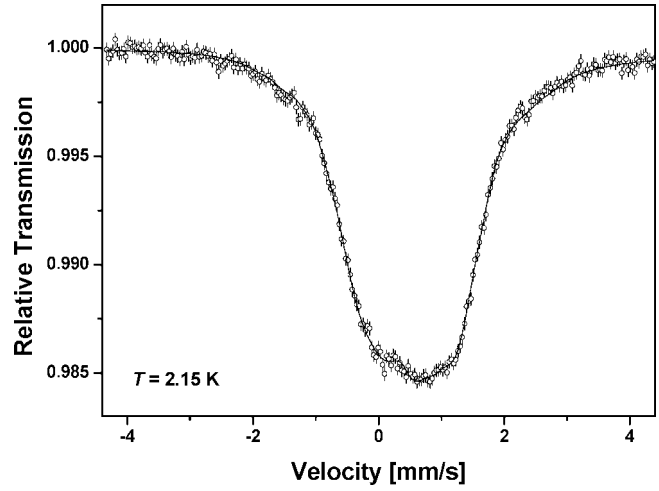

Figure 12. ^{155}Gd resonance spectrum for $GdRu_2SiC$ at $T = 2.15$ K. The continuous line represents the least-squares fit to the experimental points.

sion presented in literature for GdPdCd,[39] one can show that in the above-mentioned approximation $H_{CE} = H_{hf} - H_{CP}$, where $H_{CP} = -340(20)$ kOe[40,41] is the field due to core polarization by the local 4f moment. Considering these points, one finally obtains a positive $H_{CE} = H_{hf} - H_{CP} = -304$ kOe $-$ $(-340$ kOe$) = 36$ kOe.

The Mössbauer studies can be then summarized as follows. The resonance spectra taken below and above the magnetic transition temperature, except of that measured at $T = 2.15$ K, can be consistently fitted with one unique set of hyperfine parameters for one main component. This means that the $GdRu_2SiC$ sample is essentially single phase in agreement with XRD powder data. The resonance line-width is close to the natural width, pointing to a high homogeneity of the $GdRu_2SiC$ sample. Careful analysis of the Mössbauer spectra shows a collinear magnetic arrangement along the **a**-axis at low temperatures. In contrast to the spectra recorded at and above 4.2 K, the spectrum obtained at $T = 2.15$ K has completely different shape (Figure 12), and can not be well-described in terms of a single magnetic component. However, this spectrum could be effectively fitted assuming a distribution of magnetic hyperfine fields. After applying a multicomponent analysis, it was possible to describe the spectra accurately. An approach of the Wivel and Mørup method[26] has been applied. Because of a rather poor resolution of the ^{155}Gd spectroscopy, our fits were made in this case with the constrained values of polar angles θ and φ to those derived from the 4.2 K spectrum. The derived probability distribution curve $F(H_{hf})$ is shown in Figure 13. This distribution can be composed of five subsets, although the last one has rather small intensity and can be an artifact of the fitting procedure. Hence, the first four subsets can be tentatively prescribed to four possible magnetic components discussed above. The shapes of these individual components can be well-fitted by Gaussian distribution. The fact that the average value of the magnetic hyperfine field $H_{hf} = 292(3)$ kOe evaluated for the discussed distribution fit to the Brillouin function in Figure 11 seems to be not accidental by supporting the applied method of numerical analysis.

The observed distribution of magnetic hyperfine fields manifests that the magnetic structure of $GdRu_2SiC$ changes dramatically below $T = 4.2$ K. In view of previous discussion, it is clear that below 4.2 K the magnetic moments deviate from the **a**-axis and the derived distribution points to the magnetic ordering of a noncollinear character.

It is worth noting that the isomer shift is almost constant in the whole temperature range, in a good approximation, to the value δ_{IS} (4.2 K) $= 0.52(1)$ mm/s.

(39) Hoffmann, R.-D.; Pöttgen, R.; Fickenscher, Th.; Felser, C.; Łątka, K.; Kmieć, R. *Solid State Sci.* **2002**, *4*, 609.
(40) Watson, R. E.; Freeman, A. J. Hartree−Fock Theory of Electric and Magnetic Hyperfine Interactions in Atoms and Magnetic Compounds. In *Hyperfine Interactions*; Freeman, A. J., Frankel, R. B., Eds.; Academic Press: New York, 1967; p 53.
(41) Gegenwarth, R. E.; Budnick, J. I.; Skalski, S.; Wernick, J. H. *Phys. Rev. Lett.* **1967**, *18*, 9.

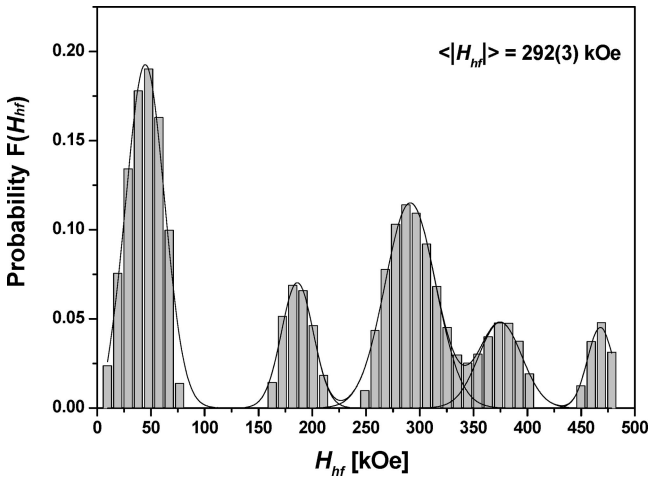

Figure 13. Field distribution function $F(H_{hf})$ obtained for the ^{155}Gd spectrum of $GdRu_2SiC$ recorded at $T = 2.15$ K. Solid lines denote Gaussian profiles fitted to the distribution.

Summary

Quaternary silicide carbide $GdRu_2SiC$ crystallizes with the orthorhombic $DyFe_2SiC$ type structure. The ruthenium, silicon, and carbon atoms build up a complex three-dimensional $[Ru_2SiC]$ polyanionic network in which the gadolinium atoms fill distorted channels. The main feature of the chemical bonding is the very strong bonding interaction within the polyanionic network. The strongest bonding has been found between ruthenium and carbon. Both the bonding distance and the size of the covalent contribution to the band-structure energy suggest double-bond character. Together with the attractive Ru−Si interactions, it is this Gd-containing network, which is responsible for the stability of the compound.

Magnetic measurements together with ^{155}Gd MS studies revealed that $GdRu_2SiC$ orders antiferromagnetically at the Neél temperature $T_N = 10(1)$ K. MS results are consistent with the model of a collinear magnetic structure in the temperature region $4.2\ \text{K} \leq T \leq T_N$, whereas a drastic change in the magnetic ordering below 4.2 K to a noncollinear one is signalized by a distribution of magnetic hyperfine fields observed at $T = 2.15$ K. A careful analysis of the magnetically split gadolinium MS spectra leads to the conclusion that in the region below T_N down to 4.2 K, the Gd magnetic moments directions are at or close to the **a**-axis, i.e., along the V_{xx} axis of the EFG tensor, whereas V_{yy} and V_{zz} remain in the basal **bc**-plane.

Acknowledgment. We thank H.-J. Göcke for the work at the scanning electron microscope and Dipl.-Ing. U. Ch. Rodewald for the intensity data collection. This work was supported by the Degussa-Hüls AG and the Deutsche Forschungsgemeinschaft through the priority programme SPP 1166 *Lanthanoidspezifische Funktionalitäten in Molekül and Material*.

Supporting Information Available: Crystallographic information (CIF). This material is available free of charge via the Internet at http://pubs.acs.org.

CM7020406